Machine learning techniques for estimating the individual three-dimensional ground reaction forces during rugby scrummaging

Zoé Pomarat, Jean-Charles Passieux, John-Eric Dufour, Bruno Watier

Highlights

Machine Learning techniques for estimating the individual three-dimensional ground reaction forces during rugby scrummaging

Zoé Pomarat, Jean-Charles Passieux, John-Eric Dufour, Bruno Watier

- Instrumented insoles allow 3D-GRF estimation in flexed and high-horizontal-load contexts.
- Personalized Machine Learning models improve force prediction accuracy.
- The method shows accurate results across different rugby scrum phases (impact, foot repositioning, sustained pushing).
- The approach is suitable for other sports with high horizontal and flexed-foot loads.

Machine Learning techniques for estimating the individual three-dimensional ground reaction forces during rugby scrummaging

Zoé Pomarat[a,b,c,*], Jean-Charles Passieux[b], John-Eric Dufour[b], Bruno Watier[a]

[a] *LAAS-CNRS, Université de Toulouse, CNRS, UPS MS2M, Institut Clément Ader, Université de Toulouse, Toulouse, France*
[b] *Institut Clément Ader, Université de Toulouse, INSA/ISAE/Mines Albi/UPS, CNRS, Toulouse, France*
[c] *Stade Toulousain Rugby, Toulouse, France*

Abstract

Rugby scrummaging represents a critical phase of play, with its outcomes closely associated with overall match performance. Scrum success is primarily determined by the forward-directed horizontal force generated by the entire pack. Previous studies have focused either on the total force produced by the pack or on individual efforts against a scrum machine. To evaluate the contribution of each player to horizontal force production within a live scrum, portable measurement systems are required. Instrumented insoles offer a field-based solution for measuring ground reaction forces (GRF). However, they are generally limited to measuring only the perpendicular component of force to the insole surface, for situations involving mainly vertical GRF, with flat-foot contact. The objective of this study was to compare the performance of four Machine Learning algorithms (Random Forest, Multi-Layer Perceptron (MLP), Long-Short-Term Memory, and a combination of a Long-Short Term Memory and an MLP) for estimating the three-dimensional GRF during rugby scrummaging using instrumented insoles. Various training configurations were tested, including dataset expansion through the merging of two experimental datasets and the application of model personalization. The best results were obtained using a personalized MLP trained on the reduced dataset, yielding root mean square error values normalized by body weight of 1.8 ± 0.3 % (Medio-Lateral), 5.6 ± 1.1 % (Antero-Posterior), and 8.3 ± 2.2 % (Vertical). The non-personalized MLP model trained on the extended dataset also demonstrated strong performance, indicating its suitability for application to new individuals with minimal reduction in accuracy.

Keywords: Biomechanics, Rugby Union, Force Estimation, Wearable Technologies, Artificial Intelligence

*Corresponding author.
Email address: zpomarat@laas.fr (Zoé Pomarat)

Figure 1: Rugby scrummaging during a rugby game. The two packs of forward players of each team compete for the ball introduced by the scrum-half (credit: Stade Toulousain Rugby).

1. Introduction

Rugby scrummaging (Figure 1) constitutes a critical phase of the game, with its outcome closely correlated with overall match result (Bennett et al. (2021); Scott et al. (2023); Vaz et al. (2019)). The forces generated by the eight players of the entire pack are substantial, particularly in the forward horizontal direction, and are a key determinant of scrum success. Therefore, many researchers have investigated horizontal force production, at the level of individual players (Green et al. (2017a); Green et al. (2017b); Lallemand et al. (2020); Milburn (1990); Milburn (1993)), the entire pack (Preatoni et al. (2016); Quarrie and Wilson (2000)) or specific positions or lines within the pack (Du Toit et al. (2004); Du Toit et al. (2005)), primarily using scrum machines. However, such machines often overestimate forces due to their rigid structure, and the forces measured may not reflect those produced in live scrummaging (Green et al. (2019)). Notably, machine-based scrums exclude ball engagement and fail to replicate the instability of an opposing pack. To better replicate match conditions, some researchers have used shoulder-mounted pressure sensors to measure individual front-row forces during live scrums (Cazzola et al. (2013); Preatoni et al. (2016)). However, these sensors often underestimate force due to limited shoulder coverage (Preatoni et al. (2016)). Additionally, no study has yet quantified each player's contribution to total scrum force, highlighting the need for individualized force measurements under real-world conditions.

The gold standard for measuring ground reaction forces (GRF) is the force plate.

Instrumenting sixteen moving feet with rigid, costly equipment is impractical. Model-based approaches like Inverse Optimal Control have been proposed to estimate GRF by identifying optimal cost weights underlying an optimal motion (Weng et al. (2022)), but their bi-level formulation is computationally intensive and susceptible to local minima, limiting practical application in human motion analysis. To address these limitations and enable field measurements, more affordable and portable alternatives have been developed. These include Inertial Measurement Units (IMUs) and instrumented insoles equipped with pressure or force sensors. However, IMU-based GRF estimation typically requires a biomechanical model (Ancillao et al. (2018)), and insoles only measure force normal to their surface. Thus, researchers have integrated these tools with Machine Learning (ML) techniques to estimate three-dimensional GRF (3D-GRF), using inputs such as IMU signals (Alcantara et al. (2022); Lee and Park (2020)), insole data (Bergamo et al. (2023); Burch et al. (2023); Fong et al. (2008); Hajizadeh et al. (2023); Kammoun et al. (2024); Nagashima et al. (2019)), kinematics (Johnson et al. (2018); Komaris et al. (2019)) or their combinations (Sabbah et al. (2024)). Most ML models have focused on cyclic activities like walking, running, or manual tasks, which mainly involve vertical forces and flat-foot contact. In contrast, rugby scrummaging is characterized by significant horizontal force generation during different phases (impact, foot repositioning, sustained pushing), all involving highly flexed feet. Preliminary observations using the Loadsol Pro® insoles (Novel, Germany) suggest they may overestimate forces in this context (Figure 2). Although various ML algorithms have been explored (Bergamo et al. (2023); Kammoun et al. (2024); Sabbah et al. (2024); Slijepcevic et al. (2024); Yamaguchi et al. (2023)), few studies have examined the effects of insole flexion or model personalization (Honert et al. (2022)), especially during rugby scrummaging.

Preliminary research (Pomarat et al. (2024)) assessed the performance of a specific ML model to accurately predict the 3D-GRF during rugby scrummaging on subjects with no specific experience. The objective of the present study was to expand the research by including elite development rugby players, and comparing several ML algorithms (Random Forest (RF), Multi-Layer Perceptron (MLP), Long-Short-Term-Memory (LSTM), and a combination of an LSTM and an MLP (LSTM-MLP)), with and without model personalization, to identify the best trade-off between performance and computational cost for estimating 3D-GRF with instrumented insoles during rugby scrummaging. RF was cho-

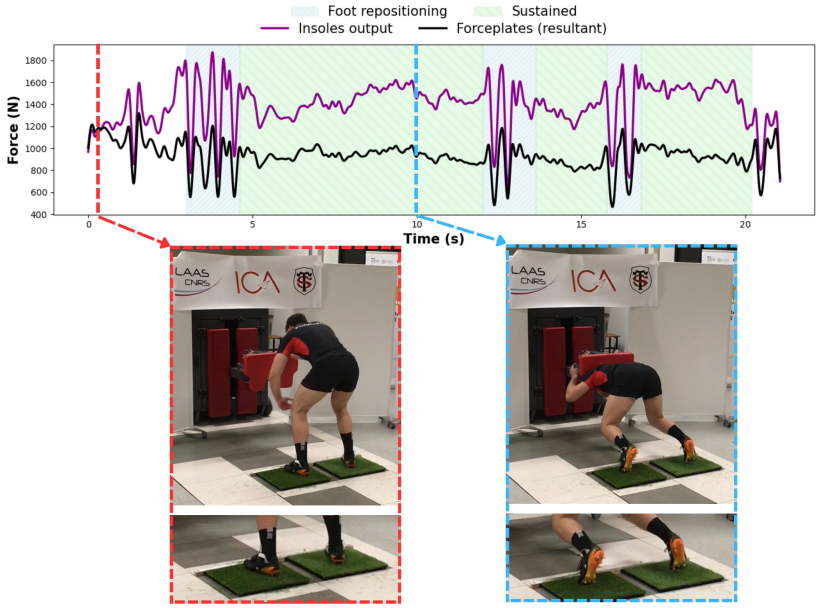

Figure 2: Overestimation of the force measured by the insoles during high flexion. The purple line represents the raw force measured by the insoles. The resultant force measured by the force plates is represented in black. When the foot remains flat (red dashed line), the force measured by the insoles is close to the resultant measured by the force plates. However, when the insole is bent within the shoe when the feet are flexed (blue dashed line), the force measured by the insoles is overestimated.

sen for its robustness to overfitting and strong generalization on small datasets, thanks to random feature selection and bootstrap aggregation (Breiman (2001)). MLP was included for its ability to capture nonlinear input-output relationships (Hornik (1991)), and LSTM for modeling temporal dependencies in sequential data (Hajizadeh et al. (2023)). It was hypothesized that the method from the preliminary study would remain effective, and that both dataset expansion and personalization would improve the ML models' performance in predicting 3D-GRF during rugby scrummaging.

2. Material and methods

2.1. Participants and data collection

Two experimental sessions were conducted. The first session involved thirteen healthy participants without specific experience in rugby scrummaging (3 females, 10 males; age: 26±6 years; height: 174±6.2 cm; weight: 71.6±11.7 kg), referred to as group 1. The second session included twelve elite development front-row rugby players from the Stade Toulousain Rugby club, experienced in performing pushing trials against a scrum machine (12 males; age: 20±1 years; height: 191±7 cm; weight: 116±13 kg), referred to

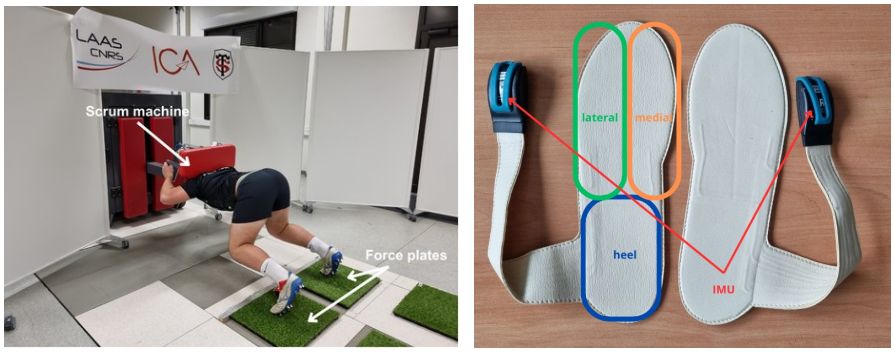

(a) (b)

Figure 3: Experimental setup (a) and instrumented insoles (b) used for this study.

as group 2. All participants were free from injuries and wore rugby shoes during testing. The experimental protocol was identical for both sessions and was approved by the Ethical Committee of the University of Toulouse (IRB No. 00011835-2024-0904-828). All participants provided written informed consent before participation.

After a self-directed warm-up, participants performed three pushing trials, each lasting 15 to 30 seconds, against a fixed scrum machine, with a five-minute rest between pushes. Participants wore commercial instrumented insoles (Loadsol Pro®, Novel, Germany) inside their rugby shoes, with each foot placed on a force plate (Sensix®, Poitiers, France) covered with artificial turf (Figure 3 (a)). The instrumented insoles comprised capacitive force sensors distributed across the insole surface, and an IMU providing 3D gyroscope and 3D accelerometer data. The insoles output three resultant normal forces, perpendicular to the insole surface, on three predefined areas: heel, medial, and lateral (Figure 3 (b)). Before each trial, the insoles were calibrated according to the instructions provided by the manufacturer. Data from the force sensors and IMU were synchronously recorded at 200 Hz using the application Loadapp (Novel, Munich, Germany). Force plate data were recorded at 1000 Hz and served as the reference for 3D-GRF measurements. Participants were instructed to perform a jump before and after each pushing trial to enable post-experiment synchronization of insole and force plate data.

2.2. Data preprocessing

Force plate and insole data were synchronized by performing a cross-correlation around the peak of vertical GRF in both signals corresponding to the first jump phase. Missing insole and IMU data, due to bluetooth connection issues and less than 0.05 s, were gap-filled using cubic interpolation. Force plate data were resampled at 200 Hz. Data were

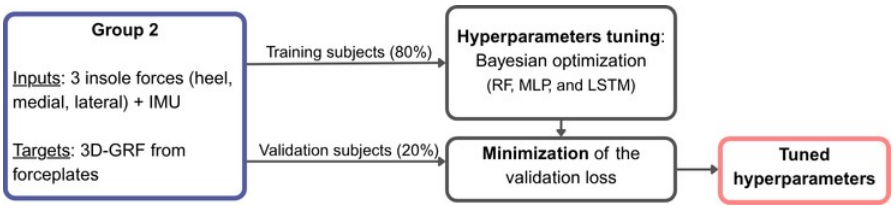

Figure 4: Overview of the hyperparameters optimization process.

filtered using a fourth-order zero-delay low-pass Butterworth filter with a cut-off frequency of 6 Hz (Cerrito et al. (2017), Fioretti (1996), Swaminathan et al. (2016), Winter (1990)). Data outside the interval between the two jumps were removed, retaining only the data related to the pushing phase.

2.3. Model architecture

Among the four supervised ML models used, the MLP, LSTM, and LSTM-MLP were implemented using Pytorch (Paszke et al. (2019)), while the RF was implemented with Scikit-Learn (Pedregosa et al. (2011)). All models used mean square error between the predicted and reference GRF as the loss function. For the MLP and LSTM models, a one-cycle cosine annealing learning rate scheduler was applied (Smith and Topin (2019)).

The architecture of the LSTM-MLP model was based on that defined in a preliminary study (Pomarat et al. (2024)). For the other models, certain parameters were considered as hyperparameters for optimization. The RF hyperparameters included the number of trees (`n_estimators`), the maximal depth of the trees (`max_depth`), and the minimum number of samples required to split a node (`min_samples_split`). For the MLP, the hyperparameters included the number of layers (`hidden_layers`), the number of nodes per layer (`hidden_dim`), the dropout rate, the maximum learning rate for the one-cycle learning rate scheduler (`LR_max`), the optimizer, the weight decay, and the batch size. The hyperparameters of the LSTM were the same as those of the MLP, with the addition of the sequence length and the direction. Various configurations of these hyperparameters (Table 1) were explored to determine the optimal architecture for each model using Bayesian optimization with Optuna (Akiba et al. (2019)). Only data from group 2 were used for the optimization process and were divided into training (80%) and validation (20%) datasets. The optimization criterion was the minimization of the validation loss. An overview of the hyperparameters optimization process is presented in Figure 4.

RF	MLP	LSTM
`n_estimators`: 50, 100, 200	`hidden_layers`: 1, 2, 3	`hidden_layers`: 1, 2, 3
`max_depth`: 10, 20, 30	`hidden_dim`: 10, 15, 50, 100, 150, 200	`hidden_dim`: 10, 15, 50, 100, 150, 200
`min_samples_split`: 2, 5, 10	`dropout`: 0.2 to 0.5	`dropout`: 0.2 to 0.5
	`LR_max`: 10^{-6} to 10^{-1}	`LR_max`: 10^{-6} to 10^{-1}
	`optimizer`: SGD, Adam, AdamW	`optimizer`: SGD, Adam, AdamW
	`weigh_decay`: 10^{-6} to 10^{-2}	`weigh_decay`: 10^{-6} to 10^{-2}
	`batch_size`: 64, 128, 256	`batch_size`: 64, 128, 256
		`sequence_length`: 50, 100, 200, 400
		`direction`: unidirectional, bidirectionnal

Table 1: Hyperparameters values explored during the Bayesian optimization for the three models to optimize.

2.4. Training

After hyperparameter tuning, several training configurations were explored, varying training dataset size (reduced or extended) and testing model personalization. Prior to splitting the data into training and test datasets, the trials of one randomly selected subject from group 2 (elite rugby players) were set aside for final validation. Among the remaining 11 subjects of group 2, one subject was randomly selected , and their three trials constituted the test dataset. The composition of the training dataset depended on the configuration. In the reduced dataset condition, it included all trials from the 10 remaining subjects of group 2. In the extended dataset condition, it included these same trials together with those of the 13 subjects from group 1. In the personalization condition, two of the three trials of the test subject were removed from the test dataset and used to fine-tune the last layer of the MLP, LSTM, and LSTM-MLP models with the hyperparameters reported in Table 2. For the final validation, the three trials of the subject initially excluded were used as the test set, while the data from the previous test subject were added to the training set.

For both optimization and training steps, the inertial data from the IMUs and the three output forces from each insole served as input data for the ML models. The target data consisted of the three components of the GRF measured by the two force plates. An overview of the training pipeline is presented in Figure 5.

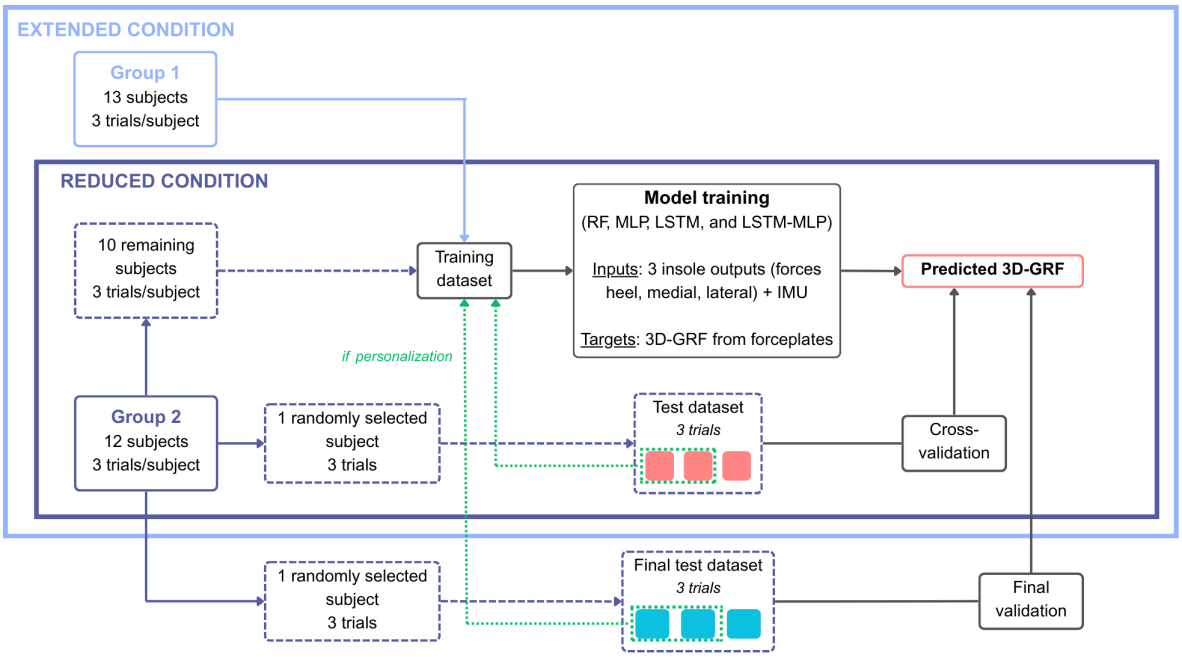

Figure 5: Overview of the training process in the different explored configurations (reduced or extended dataset, with or without personalization).

2.5. Evaluation

Due to computational cost, a partial leave-one-subject-out validation on 5 iterations was performed to evaluate the performance of the models. At each iteration, one subject from group 2 was randomly selected for validation, while the remaining subjects were used for training. Performance was assessed using the Root Mean Square Error (RMSE) between the estimated forces and the reference given by the force plates, the RMSE normalized by the test subject's body weight (RMSE%BW), and the Pearson correlation coefficient (r). The bias between the predicted and reference values for each GRF component across the entire trial was also calculated and normalized by body weight (bias%BW). To further evaluate model performance during specific phases of rugby scrummaging, the entire trial (*global*) was divided, when possible, into three phases: during the engagement phase, when a peak of horizontal force is observed (*impact*), when the subjects replace their feet to move forward, backward or finding stability (*foot repositioning*), and finally during the sustained pushing phase (*sustained*). The same metrics were calculated for these distinct phases.

3. Results

The optimized hyperparameters for the RF, MLP, and LSTM models are presented in Table 2.

The distribution of RMSE%BW, r, and bias%BW is presented for each ML model and condition in Figure 6, focusing on the Antero-Posterior (AP) axis. These results represent the average performance across the test folds of the subject-wise cross-validation, computed for the entire trial and the specific phases described previously. Detailed values on each axis are provided in Tables A.3, A.4, A.5, and A.6 in Appendix A.

RF	**MLP**	**LSTM**
`n_estimators`: **200**	`hidden_layers`: **2**	`hidden_layers`: **1**
`max_depth`: **10**	`hidden_dim`: **[200, 100]**	`hidden_dim`: **15**
`min_samples_split`: **10**	`dropout`: **0.3**	`dropout`: **0.5**
	`LR_max`: **0.0006**	`LR_max`: **0.006**
	`optimizer`: **AdamW**	`optimizer`: **SGD**
	`weigh_decay`: **3x**10^{-5}	`weigh_decay`: **0.0015**
	`batch_size`: **256**	`batch_size`: **256**
		`sequence_length`: **50**
		`direction`: **bidirectionnal**

Table 2: Hyperparameters values given by the Bayesian optimization for the RF, MLP, and LSTM models.

The MLP model trained on the reduced dataset with personalization achieved the lowest RMSE%BW across most axes and phases. Over the entire trial, RMSE%BW were 1.8 ± 0.3 % on the Lateral (L) axis, 5.6 ± 1.1 % on the AP axis, and 8.3 ± 2.2 % on the Vertical (V) axis. This condition also yielded the highest correlation coefficients with values of 0.863 ± 0.020 (L), 0.881 ± 0.044 (AP), and 0.755 ± 0.134 (V). The model exhibited a slight underestimation of the AP-GRF and a slight overestimation of the V-GRF, with biases normalized by the body weight of 0.1 ± 0.1 % (L), -0.5 ± 0.6 % (AP), and 0.7 ± 0.5 % (V). Additionally, the MLP model trained on the reduced dataset showed low variability across all phases and metrics, except for the correlation coefficient during the sustained phase.

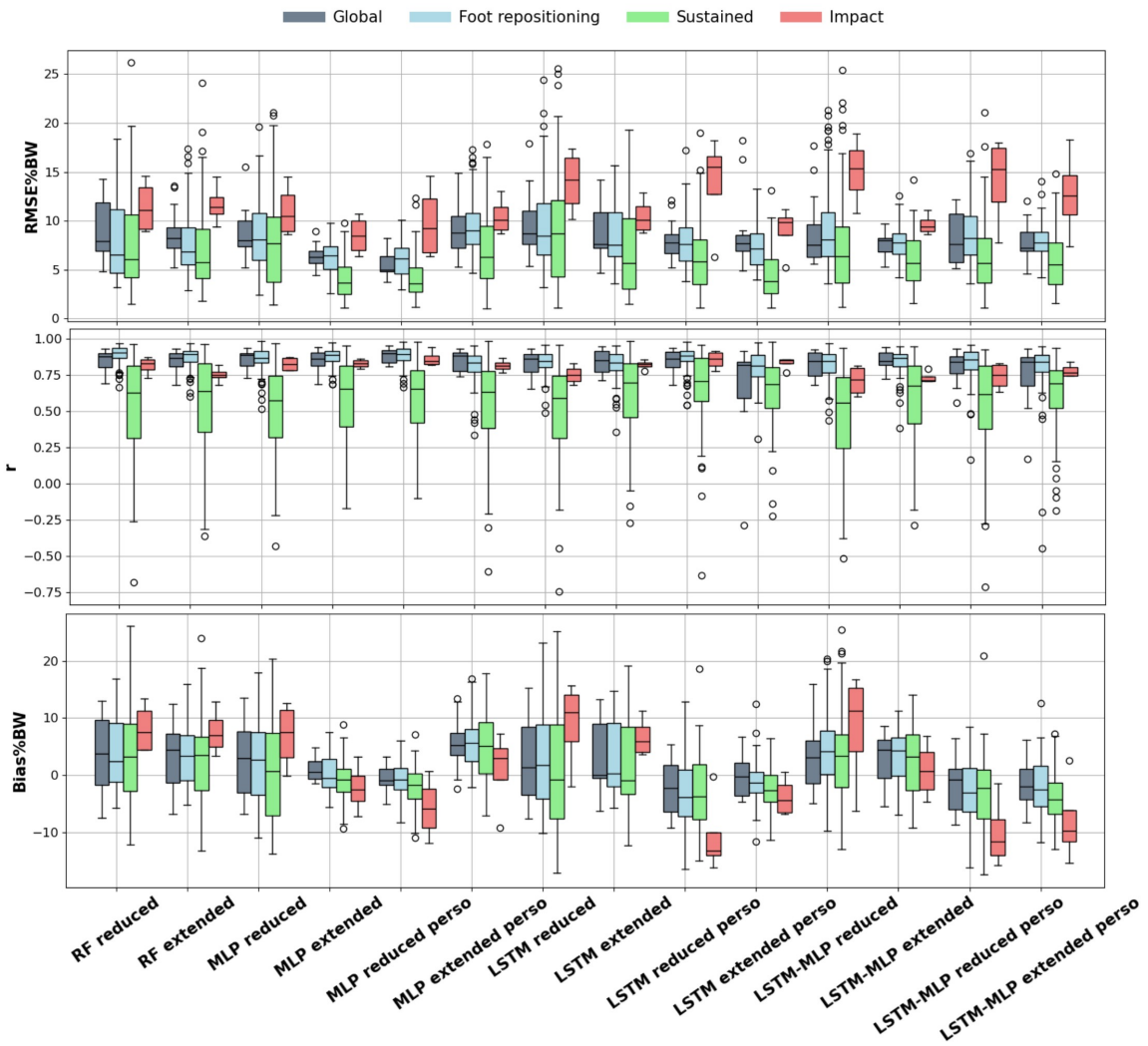

Figure 6: Distribution of the average percentage of RMSE%BW, r and bias%BW across the test folds of the subject-wise cross-validation on the entire test trial (global) and on the foot repositioning, sustained, and impact phases.

The MLP model trained on the extended dataset produced the second lowest RMSE%BW across most axes and phases. Over the entire trial, the RMSE%BW values were 2.0 ± 0.3 % (L), 6.4 ± 0.4 % (AP), and 9.4 ± 2.0 % (V). In this condition, the correlation coefficients across the entire trial were 0.849 ± 0.029 (L), 0.847 ± 0.061 (AP), and 0.723 ± 0.107 (V). The corresponding bias%BW values were 0.1 ± 0.5 % (L), 1.0 ± 1.2 % (AP), and -1.0 ± 4.8 % (V).

The LSTM model trained on the extended dataset with personalization, as well as the LSTM-MLP model trained on the extended dataset, also exhibited low RMSE%BW, high correlation coefficients, and low bias%BW values. Moreover, both models demonstrated

lower variability across all metrics during the impact phase on the AP axis compared to the two previously described models.

Extending the training dataset improved RMSE%BW and bias%BW across nearly all axes, phases, algorithms, and conditions, while also reducing result variability. A similar improvement was observed when personalizing the reduced dataset. For the LSTM and LSTM-MLP models, personalizing the extended dataset enhanced RMSE%BW, bias%BW, and reduced variability across most axes and phases. However, for the MLP model, personalization of the extended dataset had the opposite effect.

The mean forward-directed horizontal force of the subjects used in cross-validation was 502 ± 100 N during the sustained phase. Using the MLP reduced personalized model, the RMSE of the estimated force was 44.9 ± 12.0 N, corresponding to 8.9 ± 1.0 % of the mean pushing force during that phase.

Figure 7 shows an example of the 3D-GRF predicted by four models (MLP extended, MLP reduced personalized, LSTM extended, and LSTM-MLP extended personalized), compared to the reference, over an entire trial for the final test subject. The figure also shows a close-up of a foot repositioning and a sustained phase.

4. Discussion

This study aimed to compare ML algorithms and training strategies for estimating 3D-GRF using instrumented insoles during rugby scrummaging. To improve performance, two approaches were tested: model personalization when supported by the model, and dataset expansion with additional subjects, including individuals without rugby experience. Although inference was performed on male subjects, the dataset expansion included both female and male participants, as no differences were observed between sexes in the horizontal pushing force patterns. This approach was motivated by prior findings, with Honert et al. (2022) reporting that subject-specific models yielded significantly improved performance, and Halilaj et al. (2018) emphasizing the importance of a sufficiently large and diverse subject pool to mitigate overfitting. The results of this study are consistent with both previous observations. Expanding the training dataset with the two available datasets specific to the movement led to performance improvements across all models. For example, on the AP axis over the entire trial, the RMSE%BW for the RF decreased from 9.2 ± 0.4 % to 8.8 ± 2.3 %. Similar improvements were observed for the other models with

a decrease of the RMSE%BW from 8.6 ± 2.5 % to 6.4 ± 0.4 % for the MLP, from 9.7 ± 3.4 % to 8.9 ± 2.7 % for the LSTM, and from 8.9 ± 3.6 % to 7.6 ± 1.0 % for the LSTM-MLP. Additionally, subject-specific model personalization on the reduced dataset yielded improved performance across all axes and models. For the MLP for example, RMSE%BW was reduced from 2.5 ± 0.3 % to 1.8 ± 0.3 % (L), from 8.6 ± 2.5 % to 5.6 ± 1.1 % (AP), and from 13.1 ± 6.5 % to 8.3 ± 2.2 % (V) on the entire trial. Although personalization improves 3D-GRF estimation accuracy, it adds computational cost and requires a dedicated model for each subject. In high-performance sports, this is less of a concern due to the small, stable athlete pool. However, personalized models are less flexible when assessing new athletes. In such cases, a non-personalized model may be preferable, allowing evaluation of new individuals with minimal accuracy loss.

The performance of the four best-performing algorithms in this study was consistent with results reported in the literature, even across different types of activities. Kammoun et al. (2024) compared several ML algorithms for estimating the 3D-GRF using instrumented insoles across various tasks. During walking, the lowest mean RMSE values reported for each foot were obtained with the RF, with values normalized by the average body weight of the participants of 1.06 ± 0.52 % on the L axis, 2.96 ± 1.65 % on the AP axis, and 6.75 ± 3.65 % on the V axis. The corresponding correlation coefficients were 0.864 ± 0.110 (L), 0.875 ± 0.072 (AP), and 0.976 ± 0.033 (V). Similarly, Hajizadeh et al. (2023) reported RMSE%BW values of 12.96 ± 4.98 % (L), 6.26 ± 2.52 % (AP), and 5.50 ± 2.25 % (V) on both feet for walking, and values of $19.57\% \pm 10.21$ % (L), 10.42 ± 4.75 % (AP), and 7.72 ± 2.51 % (V) for jogging. Corresponding correlation coefficients were 0.926 ± 0.062 (L), 0.983 ± 0.018 (AP), and 0.985 ± 0.010 (V) for walking, and 0.955 ± 0.021 (L), 0.964 ± 0.030 (AP), and 0.980 ± 0.019 (V) for jogging. The higher RMSE%BW observed on the AP axis in the present study compared to the literature may be explained by the greater magnitude and variability of AP forces generated during rugby scrummaging compared to walking or jogging. Lallemand et al. (2020) measured an average individual forward pushing force of 1720 ± 191 N against a scrum machine during the sustained phase. These values were higher than those observed in the present study, likely due to the fact that the subjects in their setup were able to exert maximal effort without slipping. In contrast, substantial foot slippage was frequently observed during the trials of the present study, which likely limited the subjects' ability to generate maximal

horizontal force. With the best model of this study, achieving an RMSE of 8.9 ± 1.0 % of the mean forward-directed horizontal pushing force, the corresponding absolute error would be 153 ± 2 N.

Rugby scrummaging is a non-cyclic movement that can nonetheless be divided into distinct phases, each playing a specific and critical role in the overall effectiveness of the scrum. For this reason, model performance in the present study was evaluated separately across different phases: over the entire trial (*global*), during the engagement phase (*impact*), when the subjects replace their feet (*foot repositioning*), and finally during the sustained pushing phase (*sustained*). Moreover, performance expectations of the models to estimate the 3D-GRF vary depending on the phase. For instance, during the impact and foot repositioning phases, high correlation coefficients indicate the ability of the model to accurately capture rapid changes in force, while low RMSE and bias show that the magnitude of the forces is well predicted. Across all models, correlation coefficients on the AP axis were relatively low and highly variable during the sustained phase. However, this is less critical, as force variations are smaller and slower. In this phase, minimizing RMSE and bias is more relevant for assessing model performance than achieving high correlation.

Among studies comparing RF, LSTM, and MLP models, no clear consensus has emerged regarding the most effective ML algorithm for estimating 3D-GRF. For example, Kammoun et al. (2024) reported that the Random Forest (RF) model outperformed the LSTM in predicting 3D-GRF from instrumented insoles during walking, particularly in static situations. In contrast, Slijepcevic et al. (2024) found that the LSTM model performed better than both RF and MLP when using kinematic data for GRF estimation during walking. In the present study, the best performance was observed for two configurations of the MLP model: one trained on the reduced dataset with personalization, and the other trained on the extended dataset. Nevertheless, the personalized LSTM model trained on the extended dataset and the LSTM-MLP model trained on the extended dataset showed the lowest variability in both RMSE%BW and correlation coefficient on the AP axis during the impact phase. These findings related to the impact phase should, however, be interpreted with caution, as only a limited number of test trials included an identifiable impact phase. These differences in model performance may also be attributed to the nature of the input data, which varied across studies. The results show that ML

can be used to estimate all three components of GRF, even in situations where the AP force is comparable in magnitude to the vertical force, and under phases of play where the insoles are highly flexed.

This study has some limitations. First, some participants experienced varying degrees of slipping on the artificial turf, likely reducing thrust forces during engagement and limiting impact with the scrum machine, particularly among rugby players. However, similar slipping can also occur in real scrummaging situations, depending on the type and condition of the playing surface. Second, all algorithms were trained on entire trials, with performance subsequently assessed across the different phases. However, the results indicated that certain algorithms performed better in specific phases. Therefore, future work could explore training separate models specific to each phase, or applying the most appropriate pre-trained model to each corresponding phase during inference on new datasets.

5. Conclusion

This study investigated the performance of various ML algorithms and training strategies for estimating 3D-GRF using instrumented insoles with integrated IMUs during rugby scrummaging. Results showed that a simple MLP model performed best, achieving RMSE values normalized by body weight under 8.5% across all axes, over the full trial, and during foot repositioning and sustained pushing phases. This work effectively extends previous findings to conditions involving highly flexed feet and AP forces comparable in magnitude to vertical forces. While model personalization improved estimation accuracy, it limits generalization. Alternatively, expanding the training dataset to include subjects unfamiliar with rugby scrummaging proved to be an effective strategy for enhancing generalization to new individuals with minimal performance loss. Overall, the proposed approach demonstrates that estimating individual 3D-GRF during live scrums is feasible, offering new opportunities to assess player-specific contributions to the overall horizontal pushing force in rugby scrummaging.

Acknowledgment

This research was supported by Stade Toulousain Rugby and the French National Association for Research and Technology (ANRT) through a CIFRE fellowship. The au-

thors would like to thank Pierre Escalier, Valérie Vischi-Serraz, Thierry Savio, and Virgile Lacombe for enabling the implementation of this research within the Stade Toulousain Rugby.

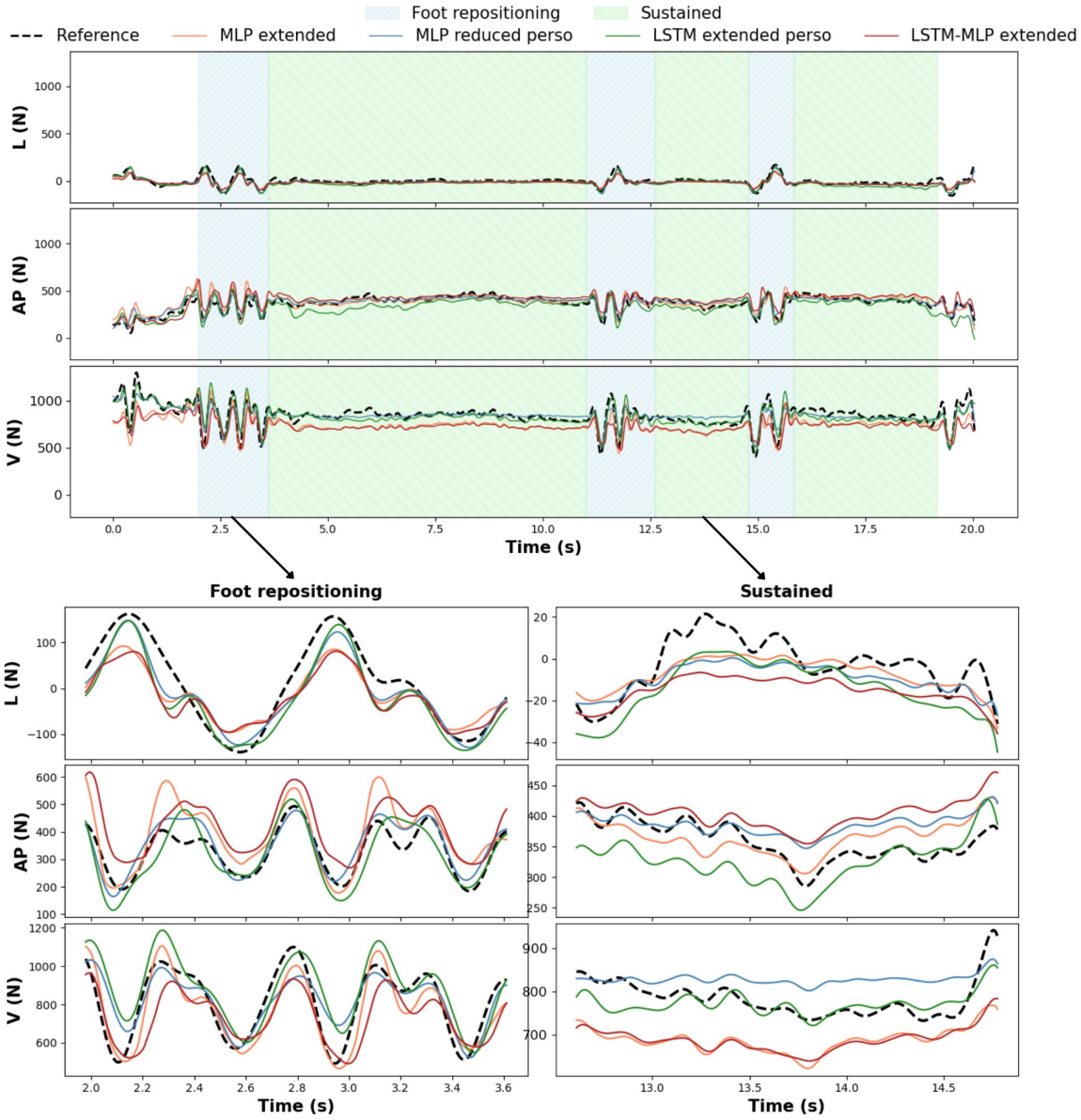

Figure 7: 3D-GRF measured by the force plates (dashed black), estimated by the MLP model trained on the extended dataset (orange), the MLP model trained on the reduced dataset with personalization (blue), the LSTM trained on the extended dataset with personalization (green), and the LSTM-MLP trained on the extended dataset (red) for an entire trial for the subject used for final testing. The blue areas represent the foot repositioning phases, and the green ones the sustained phases. The zoom on the foot repositioning phase corresponds to the first one over the entire trial, and the zoom on the sustained phase corresponds to the second one over the entire trial. There is no impact phase for this example.

Appendix A.

		Global			Foot repositioning			Sustained			Impact		
		L	AP	V	L	AP	V	L	AP	V	L	AP	V
RMSE (N)	RF	28.0 ± 5.5	103.0 ± 36.5	151.9 ± 86.7	31.9 ± 4.8	94.0 ± 47.40	137.6 ± 85.2	22.9 ± 9.9	92.9 ± 44.8	144.7 ± 115.6	26.0 ± 12.7	110.8 ± 33.6	178.0 ± 96.9
	MLP	27.7 ± 4.8	96.7 ± 30.3	145.9 ± 73.6	31.9 ± 4.4	95.3 ± 39.5	137.8 ± 70.8	22.5 ± 9.0	88.7 ± 43.4	129.9 ± 102.2	22.0 ± 2.2	107.8 ± 28.6	172.3 ± 69.0
	LSTM	28.5 ± 3.7	108.7 ± 39.4	156.4 ± 69.9	32.9 ± 2.3	109.9 ± 50.5	150.0 ± 77.8	22.6 ± 7.6	102.4 ± 53.5	139.37 ± 95.3	23.3 ± 5.7	133.6 ± 47.9	198.2 ± 75.3
	LSTM-MLP	29.8 ± 4.7	99.1 ± 40.3	147.8 ± 67.3	35.3 ± 6.0	105.4 ± 49.0	140.0 ± 68.3	23.7 ± 9.1	83.6 ± 51.2	117.3 ± 101.5	29.4 ± 12.2	153.2 ± 23.0	203.9 ± 55.8
r	RF	0.849 ± 0.042	0.853 ± 0.054	0.735 ± 0.122	0.890 ± 0.032	0.885 ± 0.033	0.887 ± 0.031	0.537 ± 0.112	0.507 ± 0.134	0.514 ± 0.099	0.434 ± 0.569	0.834 ± 0.054	0.692 ± 0.308
	MLP	0.857 ± 0.031	0.855 ± 0.056	0.733 ± 0.086	0.898 ± 0.039	0.859 ± 0.024	0.850 ± 0.027	0.619 ± 0.095	0.519 ± 0.049	0.568 ± 0.127	0.457 ± 0.649	0.810 ± 0.040	0.613 ± 0.139
	LSTM	0.842 ± 0.046	0.828 ± 0.063	0.684 ± 0.109	0.878 ± 0.062	0.830 ± 0.027	0.801 ± 0.038	0.608 ± 0.082	0.498 ± 0.060	0.436 ± 0.156	0.444 ± 0.581	0.738 ± 0.033	0.362 ± 0.044
	LSTM-MLP	0.841 ± 0.034	0.826 ± 0.067	0.686 ± 0.082	0.872 ± 0.056	0.815 ± 0.049	0.809 ± 0.066	0.616 ± 0.077	0.458 ± 0.140	0.475 ± 0.159	0.464 ± 0.301	0.687 ± 0.068	0.416 ± 0.183
RMSE %BW	RF	2.5 ± 0.4	9.2 ± 0.4	13.6 ± 7.8	2.9 ± 0.4	8.4 ± 4.2	12.3 ± 7.7	2.0 ± 0.8	8.3 ± 4.0	13.0 ± 10.5	2.4 ± 1.1	10.6 ± 2.4	16.8 ± 8.0
	MLP	2.5 ± 0.3	8.6 ± 2.5	13.1 ± 6.5	2.9 ± 0.2	8.5 ± 3.4	12.3 ± 6.3	2.0 ± 0.7	7.8 ± 3.8	11.5 ± 9.1	2.2 ± 0.4	10.4 ± 1.9	16.4 ± 5.4
	LSTM	2.6 ± 0.2	9.7 ± 3.4	14.0 ± 60.2	3.0 ± 0.2	9.8 ± 4.5	13.5 ± 6.9	2.0 ± 0.5	9.1 ± 4.7	12.3 ± 8.4	2.2 ± 0.8	12.8 ± 3.6	18.9 ± 5.8
	LSTM-MLP	2.7 ± 0.2	8.9 ± 3.6	13.4 ± 6.2	3.2 ± 0.5	9.4 ± 4.4	12.6 ± 6.2	2.1 ± 0.6	7.5 ± 4.7	10.5 ± 9.2	2.9 ± 1.4	14.8 ± 1.1	19.5 ± 3.8
Bias %BW	RF	-0.2 ± 1.7	3.7 ± 7.2	6.7 ± 11.9	-0.4 ± 1.6	4.2 ± 6.4	6.4 ± 11.8	-0.3 ± 2.0	3.2 ± 8.6	8.6 ± 14.5	-2.0 ± 1.1	7.0 ± 3.5	12.2 ± 10.5
	MLP	0.2 ± 1.6	2.4 ± 6.6	3.8 ± 11.7	-0.1 ± 1.6	3.4 ± 6.4	4.5 ± 11.2	0.3 ± 1.9	1.4 ± 8.7	3.8 ± 14.6	-1.7 ± 0.8	4.6 ± 6.6	11.7 ± 7.4
	LSTM	0.1 ± 1.6	2.5 ± 7.7	3.9 ± 11.7	-0.1 ± 1.4	3.6 ± 8.0	4.7 ± 12.4	0.3 ± 1.8	1.7 ± 10.1	3.6 ± 14.6	-1.5 ± 1.4	5.3 ± 10.3	10.4 ± 11.6
	LSTM-MLP	-0.2 ± 1.7	3.4 ± 6.3	4.8 ± 10.1	-0.3 ± 1.7	5.3 ± 6.1	5.8 ± 9.9	0.1 ± 1.9	3.4 ± 7.8	4.1 ± 13.2	-2.4 ± 1.8	3.4 ± 13.6	14.0 ± 5.7

Table A.3: Results of the cross-validation of the predicted 3D-GRF by each model compared to the reference for the reduced dataset without personalization over the different phases.

		Global			Foot repositioning			Sustained			Impact		
		L	AP	V	L	AP	V	L	AP	V	L	AP	V
RMSE (N)	RF	27.6 ± 5.3	98.2 ± 26.1	145.3 ± 72.6	30.5 ± 6.1	91.7 ± 39.0	126.4 ± 75.3	22.5 ± 9.1	84.1 ± 37.8	130.8 ± 104.3	24.8 ± 11.7	119.2 ± 15.3	161.0 ± 90.3
	MLP	22.3 ± 4.3	72.0 ± 9.6	105.5 ± 25.7	25.7 ± 7.6	69.0 ± 16.5	88.3 ± 31.4	15.7 ± 5.6	43.9 ± 13.8	67.6 ± 24.3	14.8 ± 0.5	92.1 ± 4.9	109.8 ± 9.4
	LSTM	27.2 ± 6.6	99.4 ± 31.7	151.4 ± 75.1	30.9 ± 7.0	99.1 ± 39.1	139.8 ± 63.0	21.6 ± 9.7	86.2 ± 45.7	124.9 ± 116.7	28.4 ± 0.3	103.4 ± 25.0	160.4 ± 68.7
	LSTM-MLP	27.0 ± 4.9	84.8 ± 14.3	127.2 ± 57.3	33.0 ± 8.3	86.8 ± 17.9	124.2 ± 43.4	19.5 ± 7.6	69.1 ± 16.3	103.6 ± 84.9	20.2 ± 2.9	104.6 ± 6.0	153.6 ± 22.7
r	RF	0.831 ± 0.048	0.848 ± 0.049	0.681 ± 0.165	0.889 ± 0.031	0.868 ± 0.039	0.887 ± 0.034	0.477 ± 0.106	0.530 ± 0.165	0.591 ± 0.177	0.402 ± 0.542	0.750 ± 0.002	0.654 ± 0.284
	MLP	0.849 ± 0.029	0.847 ± 0.061	0.723 ± 0.107	0.896 ± 0.036	0.870 ± 0.025	0.882 ± 0.030	0.627 ± 0.091	0.572 ± 0.076	0.597 ± 0.099	0.507 ± 0.293	0.816 ± 0.032	0.712 ± 0.098
	LSTM	0.837 ± 0.039	0.841 ± 0.059	0.664 ± 0.107	0.863 ± 0.077	0.833 ± 0.042	0.789 ± 0.060	0.577 ± 0.129	0.600 ± 0.080	0.610 ± 0.064	0.530 ± 0.288	0.819 ± 0.002	0.592 ± 0.127
	LSTM-MLP	0.827 ± 0.046	0.854 ± 0.049	0.686 ± 0.123	0.856 ± 0.062	0.838 ± 0.014	0.773 ± 0.070	0.559 ± 0.180	0.557 ± 0.114	0.546 ± 0.141	0.572 ± 0.375	0.724 ± 0.021	0.365 ± 0.125
RMSE %BW	RF	2.5 ± 0.4	8.8 ± 2.3	13.0 ± 6.5	2.7 ± 0.4	8.2 ± 3.5	11.3 ± 6.8	2.0 ± 0.7	7.5 ± 3.4	11.7 ± 9.5	2.4 ± 0.9	11.5 ± 0.6	15.2 ± 7.5
	MLP	2.0 ± 0.3	6.4 ± 0.4	9.4 ± 2.0	2.3 ± 0.6	6.1 ± 1.2	7.8 ± 2.2	1.4 ± 0.4	3.9 ± 1.1	6.0 ± 1.7	1.4 ± 0.1	9.0 ± 1.2	10.6 ± 0.0
	LSTM	2.4 ± 0.5	8.9 ± 2.7	13.6 ± 6.8	2.8 ± 0.5	8.8 ± 3.4	12.5 ± 5.6	1.9 ± 0.8	7.7 ± 4.1	11.1 ± 10.6	2.8 ± 0.2	9.9 ± 1.6	15.2 ± 5.4
	LSTM-MLP	2.4 ± 0.4	7.6 ± 1.0	11.4 ± 5.2	2.9 ± 0.7	7.8 ± 1.5	11.2 ± 4.0	1.7 ± 0.6	6.2 ± 1.5	9.3 ± 7.7	2.0 ± 0.1	10.1 ± 1.4	14.8 ± 1.0
Bias %BW	RF	-0.3 ± 1.4	3.3 ± 5.7	3.6 ± 11.2	-0.4 ± 1.5	3.8 ± 5.5	4.4 ± 10.9	-0.1 ± 2.0	2.2 ± 7.9	6.3 ± 13.9	-1.8 ± 1.1	6.9 ± 2.0	8.4 ± 12.2
	MLP	0.1 ± 0.5	1.0 ± 1.2	-1.0 ± 4.8	0.1 ± 0.6	1.1 ± 2.5	-0.6 ± 5.3	0.2 ± 0.9	-0.3 ± 2.3	0.9 ± 5.3	0.4 ± 0.4	-2.7 ± 1.4	-4.6 ± 0.5
	LSTM	-0.6 ± 1.4	3.2 ± 6.2	3.8 ± 11.5	-0.6 ± 1.3	3.5 ± 6.7	5.0 ± 10.1	-0.5 ± 1.6	2.2 ± 8.6	5.8 ± 14.2	-2.4 ± 0.1	5.6 ± 2.8	7.9 ± 11.7
	LSTM-MLP	-0.4 ± 1.2	2.0 ± 4.3	3.2 ± 8.8	-0.8 ± 0.9	3.9 ± 3.3	3.0 ± 7.9	-0.4 ± 1.3	2.2 ± 5.8	4.2 ± 11.4	-1.5 ± 0.1	-1.0 ± 5.2	3.6 ± 9.6

Table A.4: Results of the cross-validation of the predicted 3D-GRF by each model compared to the reference for the extended dataset without personalization over the different phases.

		Global			Foot repositioning			Sustained			Impact		
		L	AP	V	L	AP	V	L	AP	V	L	AP	V
RMSE (N)	MLP	20.6 ± 4.7	63.0 ± 16.4	92.4 ± 24.3	24.7 ± 7.7	66.4 ± 17.4	86.7 ± 16.2	15.6 ± 5.7	44.9 ± 13.0	49.2 ± 17.0	12.0 ± 2.3	107.0 ± 7.4	115.2 ± 24.8
	LSTM	26.0 ± 2.1	88.3 ± 17.5	134.9 ± 64.6	33.4 ± 6.4	90.9 ± 9.6	124.3 ± 47.1	19.3 ± 4.1	69.6 ± 22.8	100.3 ± 80.7	18.2 ± 4.1	150.5 ± 9.5	187.0 ± 18.0
	LSTM-MLP	25.4 ± 5.0	90.3 ± 24.0	134.0 ± 53.3	34.3 ± 8.7	93.8 ± 11.3	128.4 ± 47.9	16.5 ± 4.5	69.1 ± 12.6	95.1 ± 52.4	15.9 ± 0.8	156.1 ± 18.5	206.1 ± 6.8
r	MLP	0.863 ± 0.020	0.881 ± 0.044	0.755 ± 0.134	0.889 ± 0.051	0.876 ± 0.030	0.874 ± 0.033	0.624 ± 0.098	0.581 ± 0.051	0.544 ± 0.125	0.647 ± 0.378	0.847 ± 0.040	0.599 ± 0.325
	LSTM	0.830 ± 0.019	0.843 ± 0.056	0.698 ± 0.119	0.881 ± 0.046	0.846 ± 0.051	0.795 ± 0.092	0.632 ± 0.086	0.635 ± 0.109	0.538 ± 0.096	0.414 ± 0.224	0.868 ± 0.041	0.292 ± 0.105
	LSTM-MLP	0.823 ± 0.027	0.804 ± 0.077	0.686 ± 0.146	0.855 ± 0.061	0.811 ± 0.071	0.813 ± 0.065	0.623 ± 0.064	0.520 ± 0.119	0.531 ± 0.110	0.424 ± 0.271	0.724 ± 0.047	0.382 ± 0.057
RMSE %BW	MLP	1.8 ± 0.3	5.6 ± 1.1	8.3 ± 2.2	2.2 ± 0.6	5.9 ± 1.2	7.8 ± 1.1	1.4 ± 0.4	4.0 ± 1.0	4.4 ± 1.5	1.2 ± 0.1	10.4 ± 1.6	11.0 ± 1.5
	LSTM	2.4 ± 0.2	7.9 ± 1.3	12.0 ± 5.1	3.0 ± 0.5	8.2 ± 1.1	11.0 ± 3.3	1.7 ± 0.2	6.3 ± 2.0	8.7 ± 6.3	1.8 ± 0.6	14.6 ± 2.1	18.2 ± 3.2
	LSTM-MLP	2.3 ± 0.4	8.1 ± 2.0	12.0 ± 4.4	3.1 ± 0.7	8.5 ± 1.2	11.4 ± 3.6	1.5 ± 0.3	6.2 ± 1.4	8.4 ± 4.0	1.5 ± 0.2	15.2 ± 3.0	20.0 ± 2.3
Bias %BW	MLP	0.1 ± 0.1	-0.5 ± 0.6	0.7 ± 0.5	-0.1 ± 0.1	-0.4 ± 0.8	0.3 ± 0.8	-0.1 ± 0.4	-1.8 ± 1.2	0.2 ± 1.4	-0.1 ± 0.4	-6.6 ± 2.4	-4.0 ± 2.2
	LSTM	-0.2 ± 0.8	-2.2 ± 4.0	0.4 ± 9.0	-0.2 ± 1.0	-1.9 ± 5.8	0.3 ± 8.0	-0.3 ± 1.0	-3.1 ± 4.3	1.8 ± 10.3	1.0 ± 0.6	-11.6 ± 2.3	-12.8 ± 1.5
	LSTM-MLP	0.2 ± 0.6	-1.9 ± 3.8	-0.8 ± 8.0	0.1 ± 0.8	-1.9 ± 5.7	-1.7 ± 8.3	0.1 ± 0.6	-3.1 ± 4.1	-0.1 ± 7.9	0.6 ± 0.1	-11.2 ± 3.1	-15.2 ± 1.2

Table A.5: Results of the cross-validation of the predicted 3D-GRF by each model compared to the reference for the reduced dataset with personalization over the different phases.

		Global			Foot repositioning			Sustained			Impact		
		L	AP	V	L	AP	V	L	AP	V	L	AP	V
RMSE (N)	MLP	26.5 ± 5.2	103.7 ± 36.1	114.2 ± 29.2	28.6 ± 6.8	108.0 ± 39.9	105.6 ± 24.4	19.6 ± 9.0	85.2 ± 46.8	84.3 ± 44.6	25.8 ± 3.7	109.6 ± 4.7	108.0 ± 16.3
	LSTM	27.1 ± 4.5	97.4 ± 20.3	116.8 ± 21.1	30.8 ± 8.1	83.1 ± 17.2	111.1 ± 12.6	18.0 ± 6.2	53.2 ± 15.6	65.7 ± 31.5	18.2 ± 3.7	100.4 ± 13.4	150.5 ± 0.4
	LSTM-MLP	25.3 ± 5.6	86.6 ± 9.6	125.3 ± 21.2	32.9 ± 9.2	88.7 ± 8.3	121.4 ± 16.5	17.3 ± 6.7	64.3 ± 12.8	63.1 ± 10.8	15.4 ± 0.2	148.4 ± 42.4	141.9 ± 48.5
r	MLP	0.841 ± 0.023	0.848 ± 0.070	0.701 ± 0.108	0.894 ± 0.042	0.817 ± 0.042	0.870 ± 0.035	0.610 ± 0.080	0.532 ± 0.095	0.480 ± 0.243	0.541 ± 0.366	0.797 ± 0.047	0.756 ± 0.153
	LSTM	0.794 ± 0.073	0.691 ± 0.227	0.673 ± 0.086	0.881 ± 0.044	0.799 ± 0.035	0.780 ± 0.053	0.631 ± 0.084	0.609 ± 0.111	0.577 ± 0.064	0.577 ± 0.133	0.810 ± 0.062	0.714 ± 0.179
	LSTM-MLP	0.796 ± 0.040	0.748 ± 0.159	0.616 ± 0.106	0.654 ± 0.039	0.772 ± 0.115	0.677 ± 0.153	0.543 ± 0.100	0.599 ± 0.115	0.525 ± 0.166	0.498 ± 0.268	0.767 ± 0.033	0.644 ± 0.115
RMSE %BW	MLP	2.4 ± 0.4	9.2 ± 2.8	10.3 ± 2.9	2.6 ± 0.5	9.6 ± 3.2	9.5 ± 2.2	1.7 ± 0.7	7.6 ± 3.9	7.6 ± 4.1	2.5 ± 0.1	10.6 ± 0.4	10.4 ± 0.7
	LSTM	2.4 ± 0.2	8.7 ± 1.3	10.6 ± 2.7	2.7 ± 0.6	7.4 ± 1.1	10.0 ± 1.4	1.6 ± 0.4	4.7 ± 1.2	6.1 ± 3.5	1.8 ± 0.2	9.8 ± 2.1	14.6 ± 1.2
	LSTM-MLP	2.3 ± 0.4	7.8 ± 1.3	11.4 ± 2.6	2.9 ± 0.7	7.9 ± 0.5	10.9 ± 1.0	1.5 ± 0.5	5.8 ± 1.3	5.7 ± 0.7	1.5 ± 0.1	14.6 ± 5.3	13.6 ± 3.6
Bias %BW	MLP	-0.9 ± 0.7	5.4 ± 3.8	4.5 ± 4.5	-0.9 ± 0.8	6.3 ± 4.7	4.9 ± 3.4	-0.8 ± 0.7	5.0 ± 6.0	5.6 ± 5.6	-2.1 ± 0.1	2.0 ± 2.7	1.5 ± 3.3
	LSTM	-0.3 ± 0.6	-0.2 ± 2.7	0.7 ± 3.9	-0.3 ± 0.7	-0.4 ± 3.4	2.3 ± 4.8	-0.3 ± 1.0	-2.6 ± 2.3	2.5 ± 5.6	0.8 ± 1.0	-3.4 ± 1.3	1.4 ± 15.9
	LSTM-MLP	-0.3 ± 0.4	-1.6 ± 2.4	-1.3 ± 5.3	-0.3 ± 0.5	-1.2 ± 4.0	-0.7 ± 6.1	-0.6 ± 0.6	-3.8 ± 2.2	-0.6 ± 4.1	0.5 ± 0.1	-10.5 ± 6.9	-7.8 ± 6.9

Table A.6: Results of the cross-validation of the predicted 3D-GRF by each model compared to the reference for the extended dataset with personalization over the different phases.

References

Akiba, T., Sano, S., Yanase, T., Ohta, T., Koyama, M., 2019. Optuna: A next-generation hyperparameter optimization framework, in: Proceedings of the 25th ACM SIGKDD International Conference on Knowledge Discovery & Data Mining, pp. 2623–2631.

Alcantara, R.S., Edwards, W.B., Millet, G.Y., Grabowski, A.M., 2022. Predicting continuous ground reaction forces from accelerometers during uphill and downhill running: a recurrent neural network solution. PeerJ 10, e12752.

Ancillao, A., Tedesco, S., Barton, J., O'Flynn, B., 2018. Indirect measurement of ground reaction forces and moments by means of wearable inertial sensors: A systematic review. Sensors 18, 2564.

Bennett, M., Bezodis, N.E., Shearer, D.A., Kilduff, L.P., 2021. Predicting performance at the group-phase and knockout-phase of the 2015 rugby world cup. European Journal of Sport Science 21, 312–320.

Bergamo, G., Swaminathan, K., Kim, D., Chin, A., Siviy, C., Novillo, I., Baker, T.C., Wendel, N., Ellis, T.D., Walsh, C.J., 2023. Individualized learning-based ground reaction force estimation in people post-stroke using pressure insoles, in: 2023 International Conference on Rehabilitation Robotics (ICORR), pp. 1–6.

Breiman, 2001. Random forests. Machine Leaning 45, 5–32.

Burch, K., Doshi, S., Chaudhari, A., Thostenson, E., Higginson, J., 2023. Estimating ground reaction force with novel carbon nanotube-based textile insole pressure sensors. Wearable Technologies 4, e8.

Cazzola, D., Preatoni, E., Stokes, K., England, M., Trewartha, G., 2013. Biomechanics of rugby scrummaging: kinematic and kinetic analysis across engagement conditions, in: Book of Abstracts of the 18th Annual Congress of the European College of Sport Science in Barcelona, Spain from 26-29 June 2013, p. 249.

Cerrito, A., Evans, K., Adams, R., Pizzolato, C., Milburn, P., 2017. Kinematics of the axial skeleton during one-man rugby union scrums. ISBS Proceedings Archive 35.

Du Toit, D.E., Olivier, P.E., Buys, F.J., 2005. Kinetics of full scrum and staggered scrum engagement in under 19 schoolboy rugby union players. South African Journal for Research in Sport, Physical Education and Recreation 27, 15–28.

Du Toit, D.E., Venter, D.J.L., Buys, F.J., Olivier, P.E., 2004. Kinetics of rugby union scrumming in under 19 schoolboy rugby forwards. South African Journal for Research in Sport, Physical Education and Recreation 26, 33–50.

Fioretti, 1996. Signal processing in movement analysis (a state-space approach). Human Movement Science 15, 389–410.

Fong, D.T.P., Chan, Y.Y., Hong, Y., Yung, P.S.H., Fung, K.Y., Chan, K.M., 2008. Estimating the complete ground reaction forces with pressure insoles in walking. Journal of Biomechanics 41, 2597–2601.

Green, A., Coopoo., Y., Tee, J., McKinon, W., 2019. A review of the biomechanical determinants of rugby scrummaging performance. South African Journal of Sports Medicine 31, 1–8.

Green, A., Dafkin, C., Kerr, S., McKinon, W., 2017a. Combined individual scrummaging kinetics and muscular power predict competitive team scrum success. European Journal of Sport Science 17, 994–1003.

Green, A., Kerr, S., Dafkin, C., Olivier, B., McKinon, W., 2017b. A lower body height and wider foot stance are positively associated with the generation of individual scrummaging forces in rugby. International Journal of Performance Analysis in Sport 17, 177–189.

Hajizadeh, M., Clouthier, A.L., Kendall, M., Graham, R.B., 2023. Predicting vertical and shear ground reaction forces during walking and jogging using wearable plantar pressure insoles. Gait & Posture 104, 90–96.

Halilaj, E., Rajagopal, A., Fiterau, M., Hicks, J.L., Hastie, T.J., Delp, S.L., 2018. Machine learning in human movement biomechanics: Best practices, common pitfalls, and new opportunities. Journal of Biomechanics 81, 1–11.

Honert, E.C., Hoitz, F., Blades, S., Nigg, S.R., Nigg, B.M., 2022. Estimating running ground reaction forces from plantar pressure during graded running. Sensors 22, 3338.

Hornik, 1991. Approximation capabilities of multilayer feedforward networks. Neural Networks 4, 251–257.

Johnson, W.R., Mian, A., Donnelly, C.J., Lloyd, D., Alderson, J., 2018. Predicting athlete ground reaction forces and moments from motion capture. Medical & Biological Engineering & Computing 56, 1781–1792.

Kammoun, A., Ravier, P., Buttelli, O., 2024. Comparison of the accuracy of ground reaction force component estimation between supervised machine learning and deep learning methods using pressure insoles. Sensors 24, 5318.

Komaris, D.S., Pérez-Valero, E., Jordan, L., Barton, J., Hennessy, L., O'Flynn, B., Tedesco, S., 2019. Predicting three-dimensional ground reaction forces in running by using artificial neural networks and lower body kinematics. IEEE Access 7, 156779–156786.

Lallemand, B., Clanet, C., Blanchard, S., Noriega, P., Piscione, J., Chaplain, O., Retière, D., Cohen, C., 2020. Peak compression force physics in rugby union scrum. Proceedings 49, 151.

Lee, M., Park, S., 2020. Estimation of three-dimensional lower limb kinetics data during walking using machine learning from a single IMU attached to the sacrum. Sensors 20, 6277.

Milburn, P.D., 1990. The kinetics of rugby union scrummaging. Journal of Sports Sciences 8, 47–60.

Milburn, P.D., 1993. Biomechanics of rugby union scrummaging. Sports Medicine 16, 168–179.

Nagashima, M., Cho, S.G., Ding, M., Garcia Ricardez, G.A., Takamatsu, J., Ogasawara, T., 2019. Prediction of plantar forces during gait using wearable sensors and deep neural networks, in: 2019 41st Annual International Conference of the IEEE Engineering in Medicine and Biology Society (EMBC), pp. 3629–3632.

Paszke, A., Gross, S., Massa, F., Lerer, A., Bradbury, J., Chanan, G., Killeen, T., Lin, Z., Gimelshein, N., Antiga, L., Desmaison, A., Kopf, A., Yang, E., DeVito, Z., Raison,

M., Tejani, A., Chilamkurthy, S., Steiner, B., Fang, L., Bai, J., Chintala, S., 2019. PyTorch: An imperative style, high-performance deep learning library, in: Advances in Neural Information Processing Systems.

Pedregosa, F., Varoquaux, G., Gramfort, A., Michel, V., Thirion, B., Grisel, O., Blondel, M., Prettenhofer, P., Weiss, R., Dubourg, V., Vanderplas, J., Passos, A., Cournapeau, D., 2011. Scikit-learn: Machine learning in python. the Journal of machine Learning research 12, 2825–2830.

Pomarat, Z., Chalabi, K., Maxime, S., Dufour, J.E., Passieux, J.C., Watier, B., 2024. Estimation of ground reaction forces in rugby scrummaging using instrumented insoles and machine learning, in: 3D Analysis of Human Movement, Rehabilitation, Sports Medicine and Biomechanics, pp. 1–6.

Preatoni, E., Cazzola, D., Stokes, K.A., England, M., Trewartha, G., 2016. Pre-binding prior to full engagement improves loading conditions for front-row players in contested rugby union scrums. Scandinavian Journal of Medicine & Science in Sports 26, 1398–1407.

Quarrie, K., Wilson, B.D., 2000. Force production in the rugby union scrum. Journal of Sports Sciences 18, 237–246.

Sabbah, M., Dumas, R., Pomarat, Z., Robinet, L., Adjel, M., Watier, B., Bonnet, V., 2024. Ground reaction forces and moments estimation from embedded insoles using machine learning regression models, in: 2024 10th IEEE RAS/EMBS International Conference for Biomedical Robotics and Biomechatronics (BioRob), pp. 154–159.

Scott, G.A., Bezodis, N., Waldron, M., Bennett, M., Church, S., Kilduff, L.P., Brown, M.R., 2023. Performance indicators associated with match outcome within the united rugby championship. Journal of Science and Medicine in Sport 26, 63–68.

Slijepcevic, D., Krondorfer, P., Unglaube, F., Kranzl, A., Zeppelzauer, M., Horsak, B., 2024. Predicting ground reaction forces in overground walking from gait kinematics using machine learning. Gait & Posture 113, 214–215.

Smith, L.N., Topin, N., 2019. Super-convergence: Very fast training of neural networks

using large learning rates, in: Artificial Intelligence and Machine Learning for Multi-Domain Operations Applications, pp. 369–386.

Swaminathan, R., Williams, J.M., Jones, M.D., Theobald, P.S., 2016. Does the new rugby union scrum sequence positively influence the hooker's in situ spinal kinematics? BMJ Open Sport & Exercise Medicine 2, e000064.

Vaz, L., Hendricks, S., Kraak, W., 2019. Statistical review and match analysis of rugby world cups finals. Journal of Human Kinetics 66, 247–256.

Weng, J., Hashemi, E., Arami, A., 2022. Adaptive reference inverse optimal control for natural walking with musculoskeletal models. IEEE Transactions on Neural Systems and Rehabilitation Engineering 30, 1567–1575.

Winter, D.A., 1990. Biomechanics and Motor Control of Human Movement. John Wiley & Sons (Fourth Edition).

Yamaguchi, T., Takahashi, Y., Sasaki, Y., 2023. Prediction of three-directional ground reaction forces during walking using a shoe sole sensor system and machine learning. Sensors 23, 8985.